J Sign Process Syst (2015) 80:181–195
DOI 10.1007/s11265-013-0861-0

Biometric-oriented Iris Identification Based on Mathematical Morphology

Joaquim de Mira Jr. · Hugo Vieira Neto · Eduardo B. Neves · Fábio K. Schneider

Received: 9 May 2012 / Revised: 14 October 2013 / Accepted: 23 October 2013 / Published online: 14 November 2013

Abstract A new method for biometric identification of human irises is proposed in this paper. The method is based on morphological image processing for the identification of unique skeletons of iris structures, which are then used for feature extraction. In this approach, *local* iris features are represented by the most stable nodes, branches and end-points extracted from the identified skeletons. Assessment of the proposed method was done using subsets of images from the University of Bath Iris Image Database (1000 images) and the CASIA Iris Image Database (500 images). Compelling experimental results demonstrate the viability of using the proposed morphological approach for iris recognition when compared to a state-of-the-art algorithm that uses a *global* feature extraction approach.

Keywords Local iris features · Mathematical morphology · Biometric identification

J. de Mira Jr. · H. Vieira Neto (✉) · F. K. Schneider
Graduate School of Electrical Engineering and Applied Computer Science, Federal University of Technology – Paraná, Avenida Sete de Setembro 3165, Curitiba PR, CEP 80230-901, Brazil
e-mail: hvieir@utfpr.edu.br

J. de Mira Jr.
e-mail: mira@utfpr.edu.br

F. K. Schneider
e-mail: fabioks@utfpr.edu.br

E. B. Neves
Graduate School of Applied Biomedical Engineering, Federal University of Technology – Paraná, Avenida Sete de Setembro 3165, Curitiba PR, CEP 80230-901, Brazil
e-mail: eduardoneves@utfpr.edu.br

1 Introduction

Biometric identification is currently being used in several security applications due to increasing concerns on access control, authentication and fraud prevention. Research efforts are constantly made in order to obtain biometric recognition systems that are more efficient, secure and reliable. Besides hand geometry, fingerprint and face recognition, iris recognition in particular has been largely considered as an important field of research in biometrics.

The human iris consists of a pigmented fibrovascular tissue, formed by many minute local features – crypts, freckles, furrows and corona – which yield an arrangement rich in details. These features are unique for each individual and result from a random process in the development of anatomical structures during the embryonic stage. The iris is an externally visible organ that is stable to ageing and can be used for non-invasive biometric authentication [17, 20, 28].

Due to the great amount of local information at different scales, the use of mathematical morphology operators is a potential solution for the extraction of human iris features. Mathematical morphology is a branch of non-linear image processing that aims at extracting image information by describing its geometrical structures in a formal way. One of its main advantages is the ability to selectively preserve structural information when carrying out tasks of interest on the image.

In mathematical morphology, the information relative to the topology and geometry of an unknown set – for instance, an image – is extracted using another completely defined set called structuring element (SE) [21], which has a particular geometrical shape. The basic idea behind morphological operators is to probe the image locally in order to extract shape and size information from the way the SE geometrically fits. More complex operators (lattice operators) can be

obtained from basic operators and used to accomplish more specific tasks, such as detection of protrusions and gaps, extraction of valleys and crest-lines, feature extraction based on shape and size, among others.

This paper presents an approach based on morphological operators that is able to identify relevant local patterns in the iris for feature extraction and later classification. After feature extraction, the most stable local iris features among several image samples are selected for representation, and intra and interclass similarity distributions are established. Classification is then carried out based on these similarity distributions, aiming at obtaining an optimal decision threshold that minimises classification error rates.

Figure 1 shows the stages involved in a typical iris recognition system.

In the image acquisition stage, one of the main challenges is to set up an image acquisition hardware that is able to capture good quality images without causing discomfort to the subject under analysis. Depending on parameters such as the distance to the subject, illumination conditions and framing, a pre-processing stage may be necessary in order to improve overall image quality, highlighting iris structures and reducing reflection artifacts, for example.

In order to minimise the image area to be processed, it is necessary to determine the region of interest (ROI) between the sclera and the pupil, which comprises the iris under analysis. Automatic and robust ROI identification is not a trivial task due to factors such as low contrast between eye regions, eyelid skin pigmentation, partial eyelid occlusion and the presence of eyelashes.

After establishing the ROI, the next step concerns feature extraction. The iris is composed of many different local features, which are unique to each individual. These patterns might be represented using different methods, which are usually based on global information obtained from the Laplacian pyramid [28], multi-scale quadrature wavelets [5, 12] or zero-crossing of some wavelet transform [1, 15]. The feature representation of the iris under analysis is then finally compared to patterns stored in a database via suitable classification algorithms.

Related research explores a variety of ways to extract *global* iris features, taking into account the discriminative power that can be obtained, as well as the different stages that may be used in the process [1, 4, 5, 11, 13, 17, 19]. The novel approach presented here takes advantage of the ability of morphological operators to extract *local* information, from which the most stable features can be selected in order to represent the iris.

2 Morphology-based Iris Recognition

The human iris is composed by a variety of features that produce a structure rich in details. The basic idea of the proposed method is to apply morphological operators [21] in order to identify and highlight existing patterns in the iris, obtaining structures from which local features will be extracted and selected to build a representation. Due to diversity and quantity of spatial features of the iris, the choice of representation directly affects the amount of information to be stored.

Figure 2 presents a block diagram of the iris recognition system used in this work, which is an enhanced version of the one initially proposed in [16]. Morphological operators are used in the segmentation, morphological processing, removal of redundant pixels and feature extraction stages. Enhanced feature extraction, representation and matching stages use a new concept of stable local iris features within

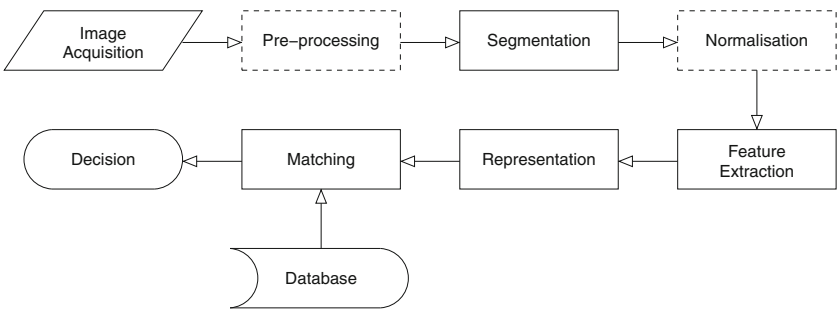

Figure 1 Typical iris recognition system. The process begins with the image acquisition of the eye, followed by an optional pre-processing stage to improve the quality of the acquired image. Next, the segmentation stage localises the inner and outer iris borders, which is followed by an optional normalisation process to compensate variations in capture distance, rotation and pupil size. The set of features known as biometric signature (iris representation) is then obtained by the feature extraction stage. In the final matching stage, iris signatures are compared and submitted to a similarity threshold in order to generate a decision.

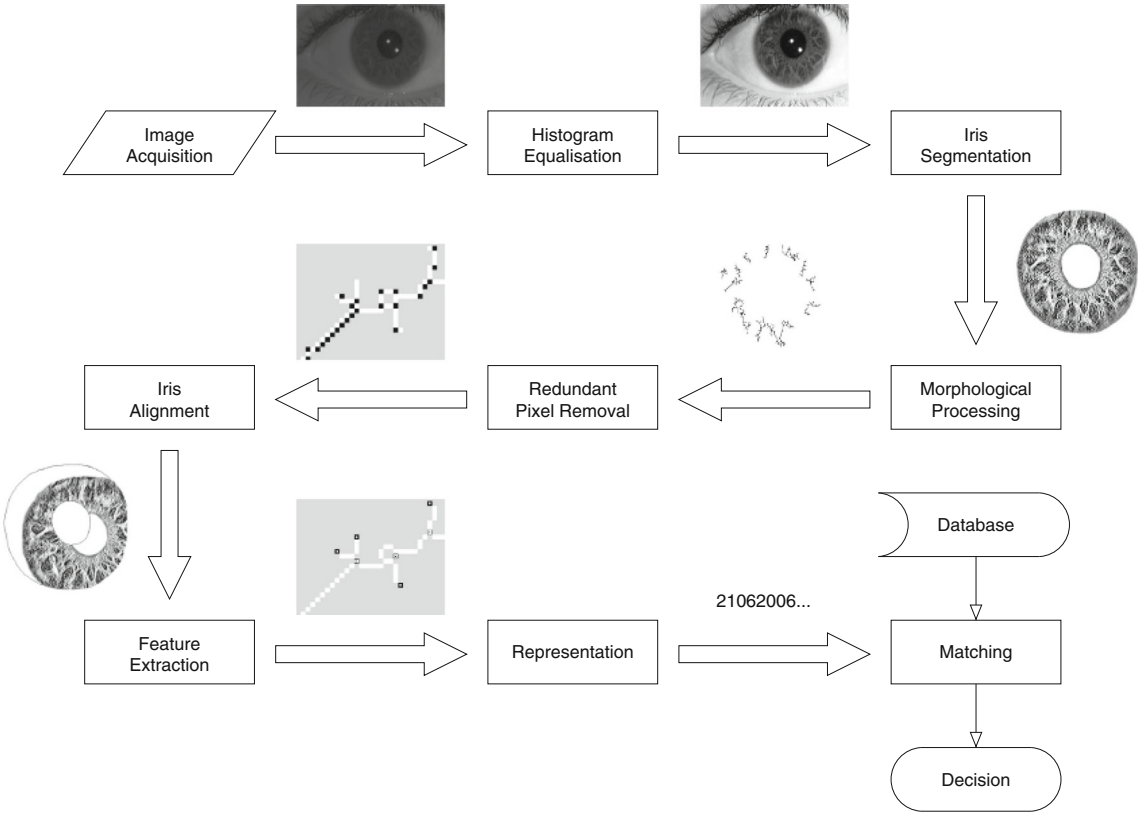

Figure 2 Enhanced morphology-based iris recognition system from previous work [16]. After image acquisition and pre-processing, a morphological iris segmentation is performed. Morphological image processing is then used in order to obtain a representation of the iris that will finally be matched to other iris representations stored in a database.

different image samples from the same subjects for the construction of corresponding reference feature vectors. The following subsections describe each stage of the system in detail.

2.1 Segmentation

After the eye image is acquired in gray-scale (8-bit resolution) and submitted to a pre-processing stage for contrast enhancement using histogram equalisation [8], it is necessary to segment the ROI containing the iris to be analysed. In order to extract the ROI – *i.e.* to identify the inner and outer borders of the iris – a sequence of operators is applied as follows.

To obtain the pupil region, which corresponds to the inner border of the iris, we first take the complement of the equalised input image. The resulting complemented image is then thresholded using a threshold value t_1 close to white (255), because after being complemented the pupil region tends to white. Some small structures and holes (noise) remaining in the resulting binary image (I_{Bi1}) are eliminated by applying an area opening operator [26] followed by a closing operator.

The area opening operator γ_λ^a removes any connected components with less area than λ in a binary image F [22, 25, 27]:

$$\gamma_\lambda^a(F) = \bigcup_{B \in A_\lambda} \gamma_B(F), \tag{1}$$

where γ_B denotes opening by structuring element B and A_λ denotes the class of subsets of a connected compact set, whose areas are greater than or equal to λ.

With the purpose to remove small structures still in the pupil region, the area opening operator defined in Eq. 1 is applied to image I_{Bi1} using a cross SE (B_C):

$$I_{Bi1}^1 = \gamma_{\lambda_1}^a(I_{Bi1}) = \bigcup_{B_C \in A_{\lambda_1}} \gamma_{B_C}(I_{Bi1}). \tag{2}$$

In order to close holes in the pupil region, the resulting binary image I_{Bi1}^1 is submitted to the closing operator ϕ_{B_B} [21, 22] using a box SE (B_B):

$$I_{Bi1}^2 = \phi_{B_B}\left(I_{Bi1}^1\right) = \varepsilon_{B_B}\left[\delta_{B_B}\left(I_{Bi1}^1\right)\right], \tag{3}$$

where ε_{B_B} and δ_{B_B} denote erosion and dilatation by structuring element B_B, respectively.

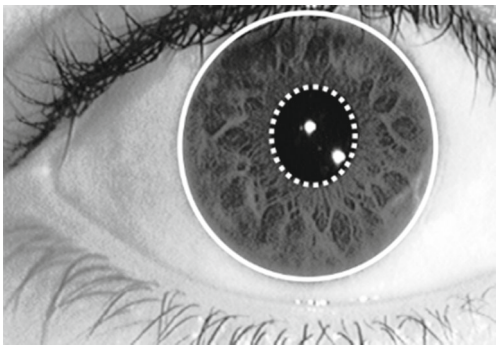

Figure 3 Iris segmentation [16]. The *inner border* (pupil) is identified by a *dotted white ellipse*, while the *outer border* (sclera) is identified by a *solid white circle*.

To detect the outer border, the previously complemented input image is thresholded considering a lower threshold value t_2 that segments the region corresponding to the iris and pupil, considering the fact that pixels of the iris region tend to appear in the middle of the gray scale. The gaps and undesired structures present in the resulting binary image (I_{Bi2}) are discarded by applying a closing operation with a box SE, followed by an area opening with a cross SE, respectively.

Figure 3 shows the result of the segmentation process just described. With information of the inner and outer iris borders, the image pixels out of the ROI can be discarded, resulting in the segmented iris image I (Fig. 4a).

2.2 Feature Extraction

After pre-processing and segmentation, a sequence of morphological operators is applied to the ROI in order to identify and enhance meaningful iris patterns to be used in further recognition or classification tasks. We conducted an investigation of the behaviour of several morphological operators when applied to existing iris patterns and their structures, in such a way to determine which operators to use and their sequence of application. Figure 4 summarises the morphological processing of the segmented ROI.

First, the segmented iris image I (Fig. 4a) is submitted to a close-by-reconstruction top-hat operator $\phi^{rec\,th}$ [22, 26] in order to highlight every existing structure. This operator creates an output image by subtracting the image I from its closing by reconstruction $\phi^{rec}_{B_{dil},B_{con}}$, defined by two structuring elements – one for dilation (B_{dil}) and other for connectivity (B_{con}). In this case a box SE was used for B_{dil} and a cross SE was used for B_{con}:

$$I_1 = \phi^{rec\,th}(I) = \phi^{rec}_{B_B,B_C}(I) - I. \tag{4}$$

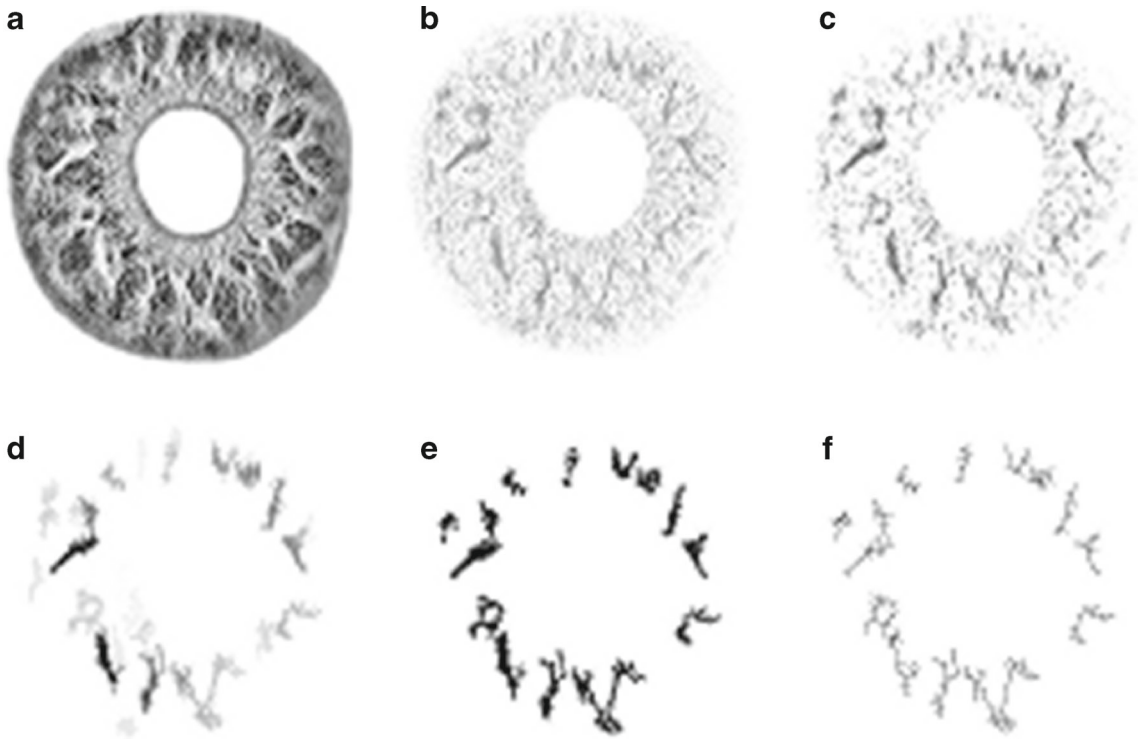

Figure 4 Morphological processing of the segmented ROI [16]. **a** segmented iris image I; **b** image I_1 with iris structures highlighted; **c** image I_2 with the most salient patterns emphasised; **d** image I_3 with small structures removed; **e** thresholded image I_4 with the most relevant structures; **f** final image I_5 with skeletonised iris structures.

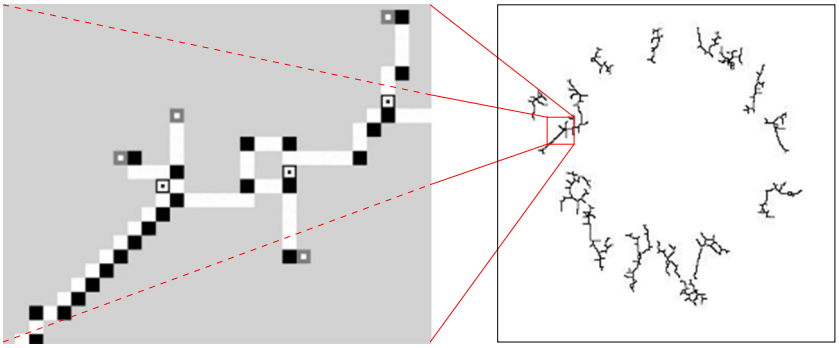

Figure 5 Detail from the skeleton of an iris structure [16]. Redundant pixels are indicated by *solid black squares*, end-points are indicated by *dark gray squares* with a central *white dot*, and nodes are indicated by *white squares* with a surrounding *black line* and a central *black dot*.

Figure 4b shows the resulting image I_1 from applying Eq. 4, where one can see that all existing iris structures are highlighted.

Next, in order to emphasise the most salient patterns in the iris, image I_1 is submitted to an opening operator γ_B using a cross SE:

$$I_2 = \gamma_{B_C}(I_1) = \delta_{B_C}\left[\varepsilon_{B_C}(I_1)\right]. \tag{5}$$

The result from applying Eq. 5 is image I_2 (Fig. 4c), where the most salient patterns (pixel arrangements of larger size) become even more evident.

In order to remove the remaining small structures of the iris, an area opening operator is then applied to image I_2. As the input image is in gray-scale, the binary version of the area opening operator is applied successively to the image layers [22, 25, 27]:

$$I_3 = \gamma^a_{\lambda_2}(I_2) = \bigcup_{B_C \in A_{\lambda_2}} \gamma_{B_C}(I_2), \tag{6}$$

using a cross SE to remove the small structures of the iris.

Figure 4d shows the resulting image I_3 from applying Eq. 6, where one can notice that small iris structures were removed.

The gray-scale image I_3 is then thresholded to segment relevant structures, yielding image I_4 (Fig. 4e). Since relevant structures appear in the dark side of the gray scale, a threshold t_3 close to black (0) is used to keep them. However, the remaining structures after thresholding still must go through a thinning process [21, 22] in order to obtain an appropriate iris representation, as these structures present themselves as agglomerates of pixels. Thinning is related to the hit-or-miss transform (HMT), which is expressed by:

$$\mathrm{HMT}_B(F) = \varepsilon_{B_1}(F) \cap \varepsilon_{B_2}(F^C), \tag{7}$$

where B_1 is the subset of B associated to the foreground, B_2 is the subset of B associated to the background and F^C is the complement of F.

In the thinning operation (THIN), each iteration is performed by subtracting points that are detected by eight hit-or-miss operators rotated by 45° from each other [8] in image I_4, as expressed by:

$$I_5 = \mathrm{THIN}_B(I_4) = I_4 - \mathrm{HMT}_B(I_4). \tag{8}$$

The final result of the thinning operation can be seen in Fig. 4f, which contains the skeleton of each relevant iris structure. However, some redundant pixels still remain in the skeletonised structures after thinning, hindering the identification of end-points and nodes, which are essential for the iris representation adopted in this work. Figure 5 shows a detail from the skeleton of an iris structure, where redundant pixels, end-points and nodes can be observed.

As can be seen in Fig. 5, there are many small details embedded in the skeleton of an iris structure that may not be significant for efficient classification. Therefore, in the method proposed here, a selection of the most stable local iris features among different image samples of the same iris is conducted in order to build a definitive reference feature vector, as detailed in Section 2.5.

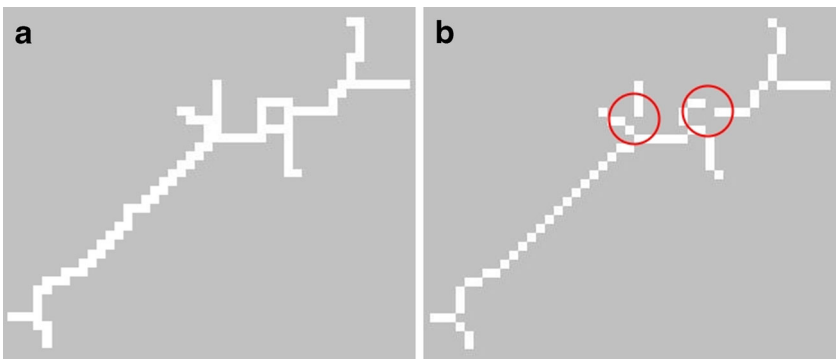

Figure 6 Results of conventional skeletonisation algorithms. **a** input image containing redundant pixels in the structure; **b** output image with undesired gaps (*highlighted with circles*) after skeletonisation.

2.3 Redundant Pixel Removal

An algorithm based on the single path concept was designed to eliminate redundant pixels from the skeleton that is obtained, resulting in a single path connecting adjacent pixels [16]. Elimination of redundant pixels must not cause any gap in the structure pattern so that local features (endpoints and nodes) are preserved. Since conventional skeletonisation algorithms often result in undesired gaps in the structure, as shown in Fig. 6, a method that verifies the neighbourhood of the pixel under analysis was designed to ensure that existing connections are preserved.

To eliminate redundant pixels, two types of 5×5 structuring elements are used: SE-1 and SE-2, shown in Fig. 7a and c, and their 90° clockwise rotated versions SE-1r and SE-2r, shown in Fig. 7b and d, respectively.

The redundant pixel removal algorithm that was developed is based on the hit-or-miss transformation, which is computed by translating the origin of the SE to each possible pixel position in the image, and comparing it to the underlying image pixels at each position. If there is a match between the SE and the underlying image pixels, the image pixel corresponding to centre of the SE is modified (in Fig. 7 these pixels are emphasised). The SE shapes were designed to verify pixels in specific neighbourhoods.

The procedure begins with a search for pixels that are set to 1 in the image. When a pixel (p) is found in this condition, the verification of its neighbourhood begins (the neighbourhood notation that was used is shown in Fig. 8). The neighbourhood verification sequence, which is related to the structuring elements used (red mask in Figs. 9 and 10), is the following:

Step 1 The centre of SE-1 (blue) is positioned over pixel N_4 in the image (Fig. 9a). If the pixels of SE-1 match the underlying pixels of the image, then pixel N_4 is set to 0 (Fig. 9b).

Step 2 The same procedure described in Step 1 is performed substituting SE-1 for SE-2.

Step 3 The centre of SE-1r (blue) is positioned over pixel N_2 in the image (Fig. 10a). If the pixels of SE-1r match the underlying pixels of the image, then pixel N_2 is set to 0 (Fig. 10b).

Step 4 The same procedure described in Step 3 is performed substituting SE-1r for SE-2r.

Steps 5 to 8 The same neighbourhood verification sequence described in Steps 1 to 4 is repeated, but now positioning the centre of the structuring elements over pixel N_3. In all cases (Steps 5 to 8), pixel N_3 will be modified if there is a match.

When the neighbourhood verification sequence (Steps 1 to 8) is finished, pixels that had their value set to 0 during the processing steps are finally modified in the output image and the image scan continues. In Figs. 9 and 10, positioning of the SE appears highlighted in red; pixels in bold correspond to positions where the SE pixels must match the underlying image pixels.

After the redundant pixel removal process, an image that is suitable for feature extraction is obtained. The result of the algorithm can be seen in the Fig. 11, where it can be noticed that redundant pixels were eliminated without causing any breaks in connection (gaps) in the structure, unlike what is observed in Fig. 6b.

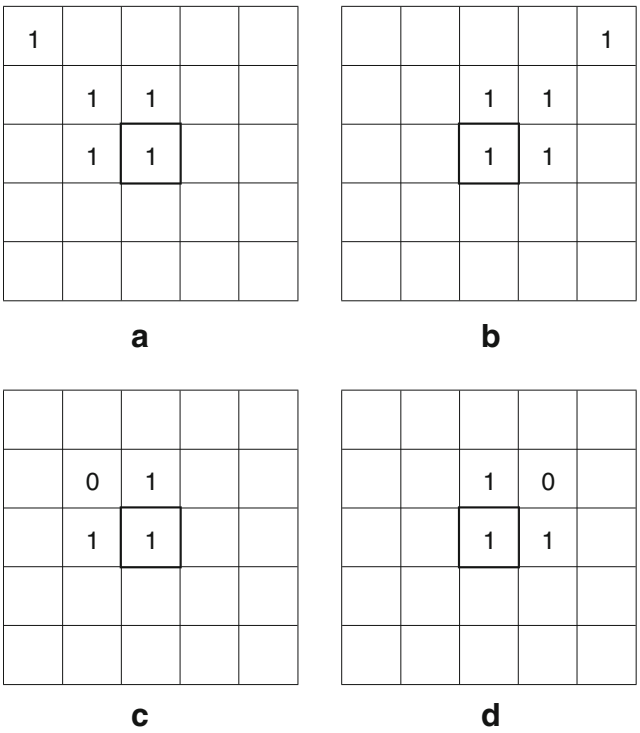

Figure 7 Structuring elements used for redundant pixel removal. **a** SE-1; **b** SE-1r; **c** SE-2; **d** SE-2r.

2.4 Geometric Normalisation

To compensate misalignments caused by translation, rotation and scaling of the iris under analysis when compared

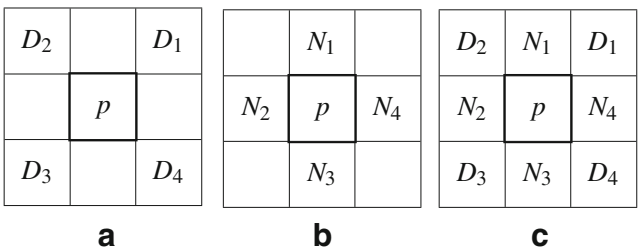

Figure 8 Neighbourhood notation that was used. **a** diagonal neighbourhood; **b** 4-neighbourhood; **c** 8-neighbourhood.

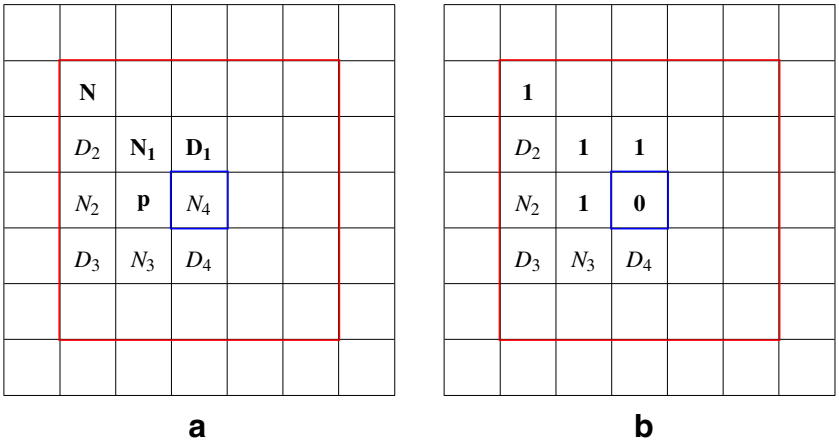

Figure 9 Step 1 of the neighbourhood verification sequence. **a** The centre of SE-1 is positioned over pixel N_4; **b** pixel N_4 is set to 0 if the pixels of SE-1 match the underlying pixels of the image.

to the images stored in the database, the binary image I_4 containing the relevant structures (Fig. 4e) is submitted to a normalisation procedure that adjusts it for the matching stage. The compensation of geometric transformation effects is done by an algorithm based on the affine motion transform [2, 23].

This procedure takes an image containing pseudo-structures as reference. Pseudo-structures are generated from the iris representation from the database, which contains the location of end-points and nodes, as shown in Fig. 12a. The binary image created from the information stored in the database is dilated twice using a box SE, in order to ensure the connectivity of each pseudo-structure, as shown in Fig. 12b, which will be used for the alignment of image I_4 (Fig. 4e) of the iris under analysis by the recognition system.

The comparison between image I_4 and the image containing pseudo-structures generated from the iris representation stored in the database allows the estimation of the error between original and actual position of features, based on the minimum absolute difference [2]. Therefore, the binary feature images can have their structures aligned for the matching procedure.

2.5 Feature Representation

The iris representation approach used in this paper is based on information about nodes (points where ramifications of the structure start), end-points (structure terminations) and branches of the structure, which can be seen in Fig. 5. After removing redundant pixels from the skeletons of the structures, the next stage consists in identifying end-points and nodes.

The identification process begins with by verifying the 8-neighbourhood of every pixel p. Since an end-point is a pixel located at the extremity of a branch, if only one neighbour of p is set to 1, then p is an end-point. Figure 13a shows examples of end-points identified in a structure. However, if three or more pixels in the 8-neighbourhood of p are set to 1, then p is considered a node. Figure 13b shows examples of nodes found in a structure. In some cases, it is necessary to eliminate redundant nodes that may appear close to each other. This redundant node removal can be performed using the following criterion: if there is more than one node within a distance of three pixels, then their average coordinates are taken as the location of the definitive

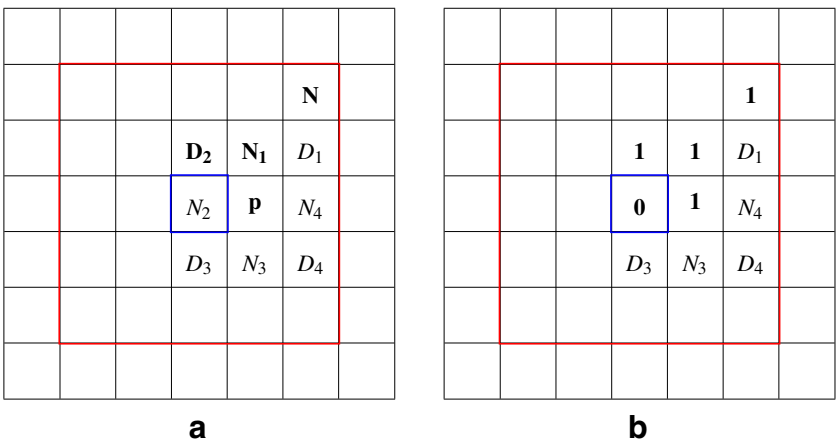

Figure 10 Step 3 of the neighbourhood verification sequence. **a** The centre of SE-1r is positioned over pixel N_2; **b** pixel N_2 is set to 0 if the pixels of SE-1r match the underlying pixels of the image.

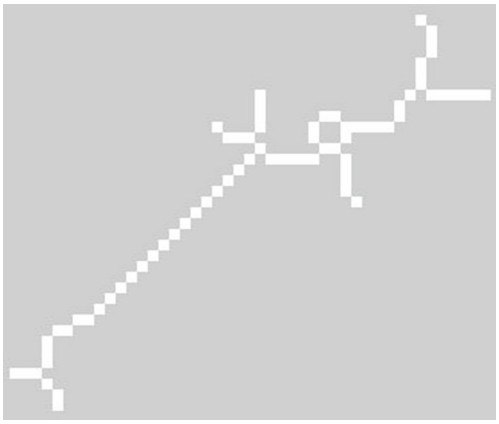

Figure 11 Result of the redundant pixel removal algorithm [16]. No gaps are present in the resulting structure skeleton (compare to Fig. 6b).

node. Figure 13c exemplifies the result of this redundant node removal criterion.

The coordinates of end-points and nodes, as well as their respective number of branches, are used to build the feature vector for iris representation. In order to obtain the number of branches for some specific node, its ramifications must be evaluated based on corresponding end-points. For each node, coordinates and number of branches are concatenated to form the corresponding feature vector.

The definitive reference feature vectors for matching are generated from the most stable local iris features present in different iris image samples per subject, in order to increase the robustness of the representation. Experiments with increasing numbers of different image samples from the same subject have shown that five feature vectors corresponding to each image sample are enough to select the most stable features in order to generate definitive reference feature vectors for each individual iris (more details are given in Section 4.2).

For the selection of the most stable local features, each of the five base feature vectors containing the coordinates of nodes is matched against all the other base feature vectors and only the nodes that are present in at least four of the five base feature vectors – the most stable ones – are selected to be included in the definitive reference feature vector. The same three pixel tolerance criterion used before for redundant node removal is used to compute average coordinates for matching stable nodes. The selection of the most stable local features for representation results in great improvement in the overall iris classification performance, as shown later in Section 4.

2.6 Matching and Classification

After mapping the coordinates of end-points and nodes, the feature comparison procedure is based on a one to one correspondence. Initially, in order to identify matching nodes, coordinates in the iris feature vector under analysis are compared to those in the reference feature vector obtained from five image samples, as described before. Then, in order to obtain the corresponding number of branches for matching nodes, the ramifications of each node are verified.

A score S is used as base parameter for the classification process and assumes normalised values in the interval [0, 1], which is computed as follows:

$$S = \frac{M}{N}, \tag{9}$$

where M denotes the number of matching nodes and N denotes the number of stable nodes in the reference feature vector.

The classification strategy adopted is based on similarity measures between classes (intra and interclass). This approach yields an optimal decision threshold T that tends to minimise the equal error rate (EER). A binary classifier for authentic and impostor identities can be established based on this optimal decision threshold. The decision (D) reached by the classifier is defined as follows:

$$D = \begin{cases} \text{authentic}, & \text{if } S \geq T \\ \text{impostor}, & \text{if } S < T \end{cases}. \tag{10}$$

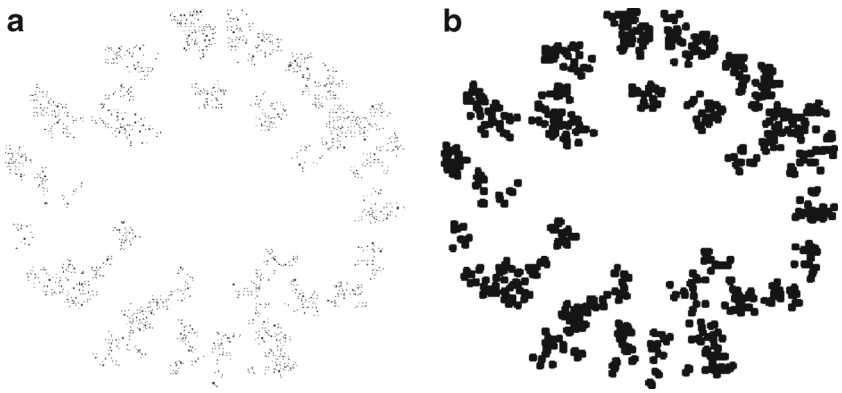

Figure 12 Reconstructed feature image [16]. **a** end-points and nodes; **b** resulting pseudo-structures.

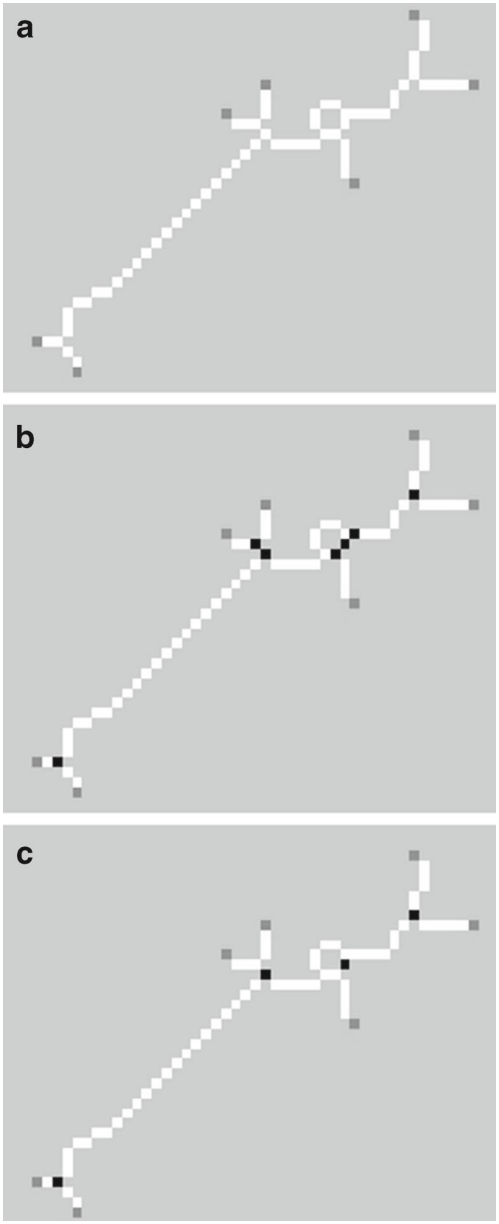

Figure 13 Feature identification example [16]. **a** identification of end-points (*dark gray*); **b** identification of nodes (*black*); **c** removal of redundant nodes.

3 Experimental Setup

A subset of 1000 images from the University of Bath Iris Image Database [24], comprising 20 images of each eye from 25 subjects, was used in order to assess the proposed iris classification method. The University of Bath Iris Image Database is composed of images of 1280 × 960 pixels in size, which were acquired in gray-scale using infra-red illumination, and was used in a number of previous studies available in the literature [9, 10, 18, 29–31].

Additionally, a subset of 500 images from the CASIA Iris Image Database V3-Interval [3], containing 10 images of each eye from 25 subjects, was also used for further assessment of the proposed method. The CASIA Iris Image Database is composed of images of 320 × 280 pixels in size, acquired in gray-scale under near infrared illumination.

In this work, five images from each subject were used to build reference feature vectors for each class, as described in Section 2.5. The remaining images from each subject were then used to test the proposed iris classification scheme. Matching between reference and test feature vectors from the databases allowed the computation of intraclass and interclass score distribution curves, which in turn were used to compute the false acceptance rate (FAR) and the false rejection rate (FRR) of the classifier and to determine an optimal decision threshold for class separation. Receiver operating characteristics (ROC) curves [14] and their respective AUC (area under the curve) and EER (equal error rate) statistics were also used for performance assessment.

The feature vectors obtained from the images for each class in the databases were submitted to a matching process so that intraclass and interclass score distribution curves and figures of merit could be computed. This procedure was used in order to perform statistical assessments of the proposed method and to allow comparisons with other methods. Therefore, all experiments were conducted in two stages, as shown in Fig. 14.

In the intraclass matching stage, for each subject in the database, the reference feature vector of each subject was matched against the test feature vectors of the same subject. In the interclass matching stage, the reference feature vector of each subject was matched against the reference feature vectors of the remaining subjects.

In order to have a baseline for comparison of the results obtained for the proposed method, the state-of-the-art iris recognition method proposed by Daugman [5–7] was also implemented and used following the experimental procedure shown in Fig. 14.

4 Results

Intraclass and interclass score distribution curves and the ROC curve for matching nodes were computed in order to assess the performance of the proposed approach for iris classification. Results obtained for Daugman's method were used to compute intraclass and interclass Hamming distance distribution curves and the corresponding ROC curve.

Figure 15 shows the intraclass and interclass matching distribution curves obtained for the method proposed in this work and Daugman's method using the subset of images from the University of Bath Iris Image Database.

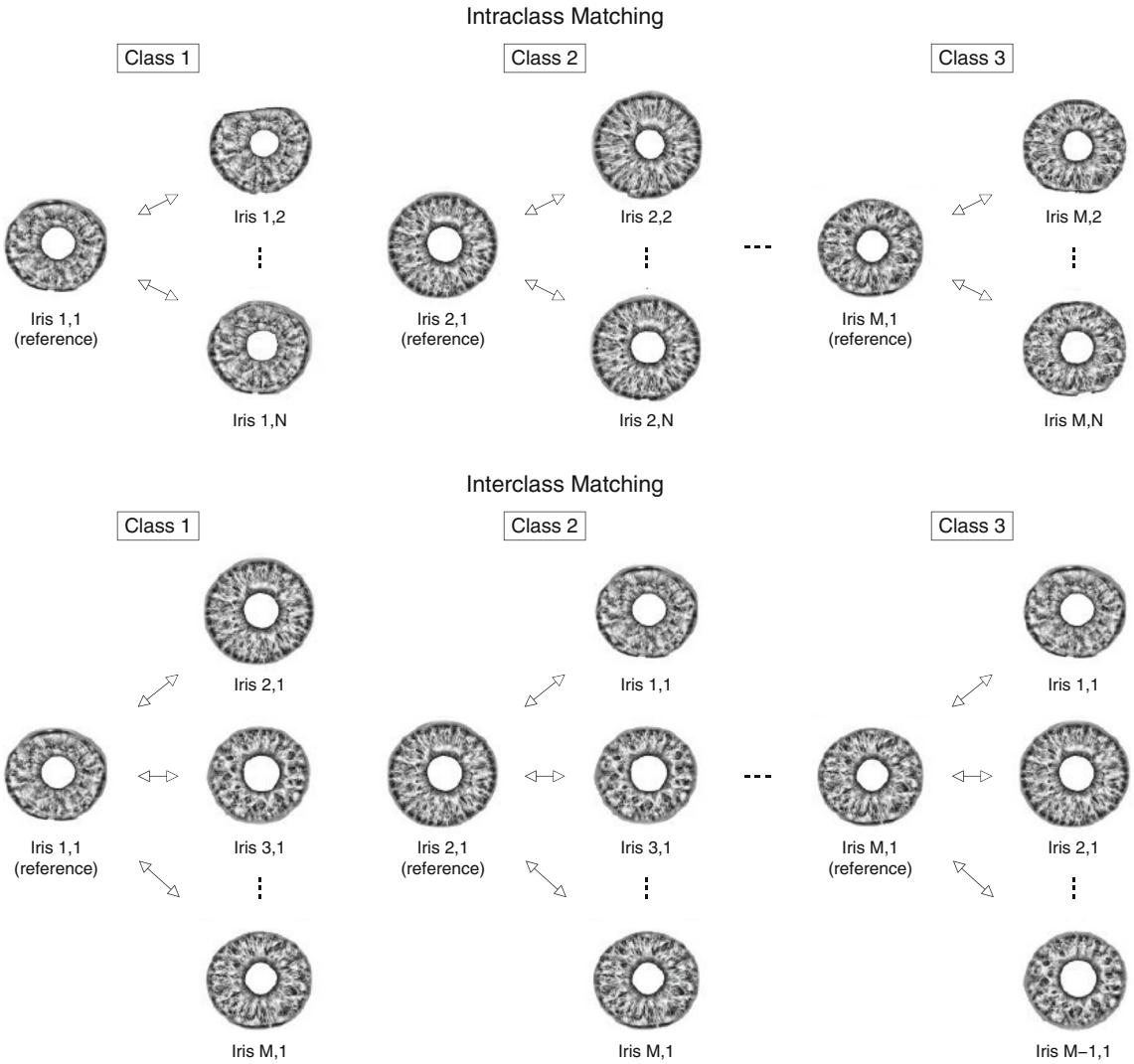

Figure 14 Intraclass and interclass statistical assessment scheme. Intraclass matching was conducted among iris samples of the same subject, while interclass matching was conducted among iris samples of different subjects.

It can be noticed from the curves in Fig. 15 that there is a clear separation between intra and interclass distributions for both methods. The distribution curves appear more widely spread throughout the similarity axis in Fig. 15a, a characteristic that seems to favour class separation and to contribute for the achievement of low error rates. In Fig. 15b the distributions curves for the Hamming distance used in Daugman's method are more concentrated in a reduced range of the dissimilarity axis.

ROC curve analysis was also used in order to compare performances. The ROC curve plots the false rejection rate (FRR) as a function of the false acceptance rate (FAR) for varying threshold values – the FAR indicates the probability of accepting an impostor and the FRR indicates the probability of rejecting an authentic subject – obtained from intraclass and interclass comparisons for each sample in the database.

4.1 Classification Using All Detected Iris Features

A first experiment to assess classification performance using all detected iris features to compose reference feature vectors (V1) was conducted with the subset of images from the University of Bath Iris Image Database. Figure 16 shows the resulting ROC curves for both proposed and Daugman's methods.

As can be seen in Fig. 16, using all local iris features to compose reference feature vectors results in worse classification performance than the one obtained using Daugman's method.

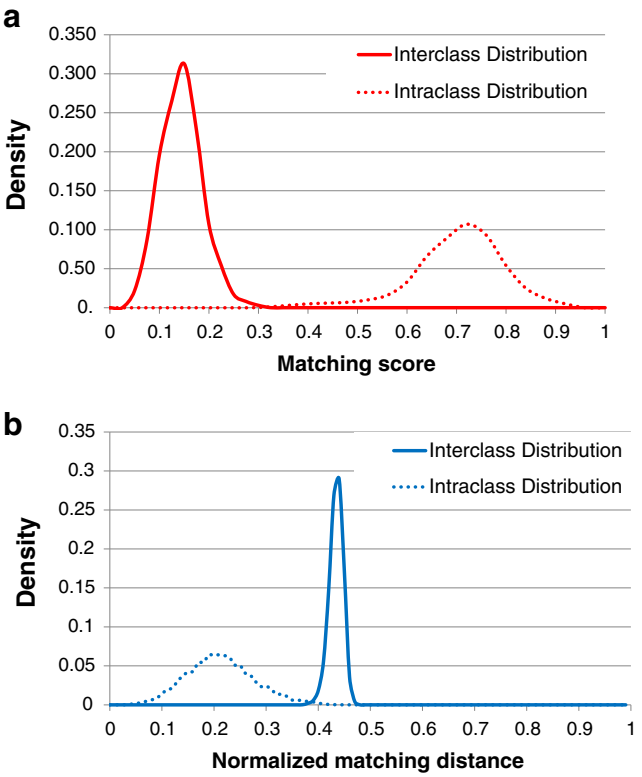

Figure 15 Intraclass and interclass matching distribution curves for the subset of images from the University of Bath Iris Image Database. **a** matching scores (proposed method); **b** matching distance (Daugman's method). Higher matching scores in the proposed method represent higher similarity between irises. Daugman's method uses the Hamming distance and therefore higher values represent higher dissimilarity between irises.

4.2 Selection of the Most Stable Iris Features

Given the first results obtained, an extra experiment was conducted in order to determine whether the selection of stable local iris features would have any positive impact in the overall classification performance of the proposed method. For that purpose, only five subjects were randomly chosen from the subset of images from the University of Bath Iris Image Database, and an increasing number of image samples – ranging from two to seven – was used to select stable features and to assess the corresponding classification performances. Figure 17 shows the ROC curves obtained for classification using an increasing number of image samples for feature vector composition using the most stable features for the same subjects.

It can be noticed in Fig. 17 that significant improvement in classification performance is obtained by using five or more image samples to select stable features. As the improvement in performance is not expressive for more than five image samples, the number of image samples for the selection of the most stable iris features was set to five.

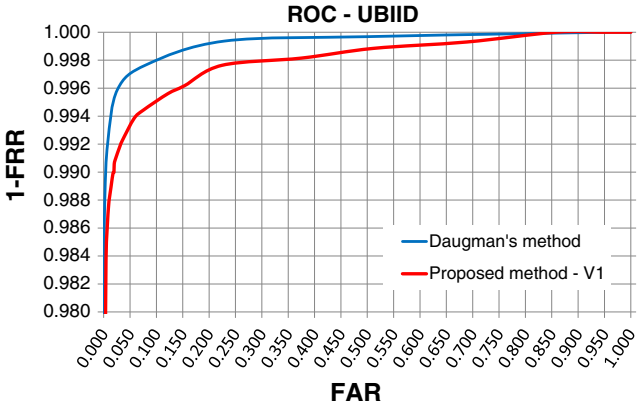

Figure 16 ROC curves obtained for both proposed method - V1 (*red line*) and Daugman's method (*blue line*) using a subset of image samples from the CASIA Iris Image Database. Composing reference feature vectors with all detected iris features results in worse overall performance of the proposed method.

4.3 Classification Using the Most Stable Iris Features

Following the encouraging results obtained in the experiment using the selection of stable local iris features, a second experiment to assess classification performance using the entire subset of images from the University of Bath Iris Image Database was conducted using this approach (V2). Figure 18 shows the results obtained, in which one can notice that the proposed method shows equivalent overall performance to the one obtained using Daugman's method when using the most stable iris features from five image samples.

Table 1 summarises typical biometric recognition system FAR configurations and their corresponding FRR taken from the ROC curves in Fig. 18. The area under the ROC curve (AUC), equal error rate (EER) and accuracy of the

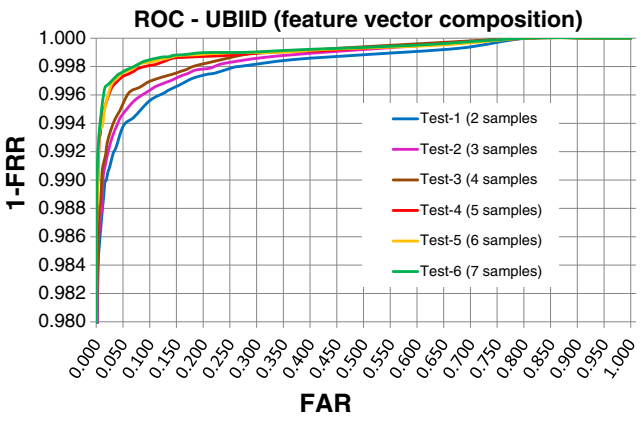

Figure 17 ROC curves obtained for an increasing number of image samples for feature vector composition using the most stable features among the samples. Selecting stable features from five or more image samples results in significant improvement in classification performance.

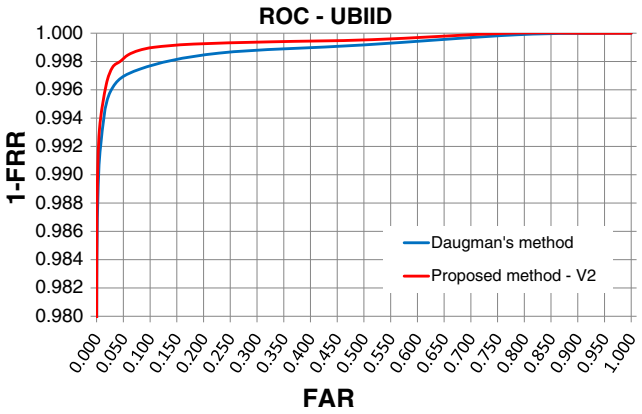

Figure 18 ROC curves obtained for both proposed method - V2 (*red line*) and Daugman's method (*blue line*), using a subset of image samples from the University of Bath Iris Image Database. When only the most stable iris features are used to compose reference feature vectors, both methods yield equivalent performances.

classifier were also used to assess the overall performance of both methods – results of these assessments are shown in Table 2 and confirm the equivalent performance yielded by both methods, indicating the feasibility of iris recognition using a local feature extraction approach based on mathematical morphology.

Additional experiments using the V2 approach were also conducted with a subset of image samples from the CASIA Iris Image Database. The results shown in Fig. 19 confirm that the proposed method yields equivalent performance to the one obtained using Daugman's method.

Tables 3 and 4 summarise the information from the ROC curves shown in Fig. 19 in terms of FAR and FRR, and also AUC, EER and classifier accuracy statistics. Slightly worse overall performances were obtained with the CASIA Iris Image Database and this fact is attributed to the much lower image resolution available in this database in comparison to the image resolution available in the University of Bath Iris Image Database.

Table 1 Typical FAR configurations and corresponding FRR obtained for both methods – subset of image samples from the University of Bath Iris Image Database.

FAR	FRR (Daugman)	FRR (Proposed)
0.1 %	0.23 %	0.11 %
0.01 %	0.71 %	0.52 %
0.001 %	1.36 %	1.16 %
0.0001 %	2.02 %	1.97 %

Table 2 Area under the ROC curve (AUC), equal error rate (ERR) and accuracy obtained for both methods – subset of image samples from the University of Bath Iris Image Database.

	Daugman	Proposed
AUC	0.99921	0.99941
EER	0.78 %	0.65 %
Accuracy	99.22 %	99.35 %

5 Discussion

Daugman's method was implemented according to information available in the literature [5–7]. The mean value of 0.46 obtained for the interclass Hamming distance distribution (see Fig. 15b) is practically the same reported in the literature, in spite of the fact that a different iris image database was used, indicating that the implementation of Daugman's method used in this work presents coherent results.

Several iris recognition methods available in the literature use Daugman's rubber-sheet homogeneous model [5] to map the iris to a dimensionless coordinate system in order to compensate changes in size and pupil dilation. That model is critically dependent on the accuracy in finding the inner and outer iris boundaries in the segmentation stage, and is also affected by non-concentricity and non-circularity of iris boundaries, which commonly happen in practice but nevertheless are disregarded by many methods. Occlusion is another important factor that affects iris boundaries – the inner boundary can be often occluded by reflections of the illumination device and the outer boundary by upper or lower eyelids. In the proposed method these problems are avoided because no constraint is imposed to boundary

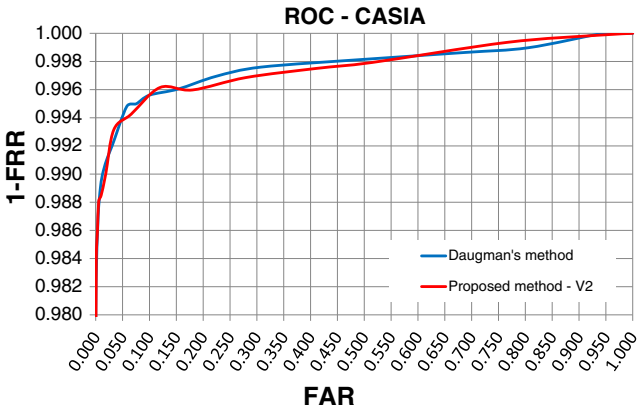

Figure 19 ROC curves obtained for both proposed method - V2 (*red line*) and Daugman's method (*blue line*), now using a subset of image samples from the CASIA Iris Image Database. Again, both methods yield equivalent performances when only the most stable iris features are used to compose reference feature vectors.

Table 3 Typical FAR configurations and corresponding FRR obtained for both methods – subset of image samples from the CASIA Iris Image Database.

FAR	FRR (Daugman)	FRR (Proposed)
0.1 %	0.44 %	0.44 %
0.01 %	1.06 %	1.15 %
0.001 %	1.66 %	1.59 %
0.0001 %	2.25 %	2.25 %

shapes by the morphological operators used in the segmentation process, which proved their efficacy to obtain the ROI.

Besides reflection and eyelid occlusion, the iris image information can also be degraded by eyelash occlusion. Eyelashes present intricate random shapes that are difficult to be detected by simple shape models and, in terms of contrast energy, can appear as the dominant signal in the iris image. If the eyelash signal is not detected and minimised, it can possibly degenerate the iris feature vector with spurious information (noise). As the proposed approach to construct iris feature vectors is based on information obtained from local iris structures and not the entire segmented iris region, eyelash occlusions tend to affect less the feature extraction process. Generally, the loss of information produced by typical occlusion caused by eyelids and eyelashes is not enough to degenerate the performance of the proposed algorithms. Due to the disposition of the structures in the iris and how the proposed algorithms process this information, the remaining areas of the iris which are free from occlusions contain enough information (stable structures) to allow comparisons still with excellent efficacy. Further studies are currently being conducted to establish the minimum percentage of occlusion-free area that is necessary to perform comparisons without compromising classification performance.

In order to compensate translation, rotation and scaling effects during image acquisition, as well as variations in pupil size, the segmented iris region is submitted to a normalisation procedure. Several approaches use the normalisation method proposed by Daugman [5], but the method proposed in this paper uses information directly from existing structures in the iris image to compensate for variations and misalignments. The normalisation procedure based on mathematical morphology that is responsible for alignment of iris structures spends about 80 % of the total processing time of the proposed iris identification algorithm. Alternatives to reduce the computational cost of this important processing stage are being currently studied and so far it was possible to establish that the images in which more time was spent for alignment also resulted in higher FRR values. Further analysis of these special cases indicates that large variations in pupil diameter between reference and candidate iris images is the most critical aspect to be looked into.

Table 4 Area under the ROC curve (AUC), equal error rate (EER) and accuracy obtained for both methods – subset of image samples from the CASIA Iris Image Database.

	Daugman	Proposed
AUC	0.99766	0.99757
EER	1.05 %	1.12 %
Accuracy	98.95 %	98.88 %

The proposed representation of iris structures based on stable nodes showed to be adequate to characterise the existing patterns in human irises, achieving excellent identification performance. The resulting representation is also compact – feature vectors obtained using the proposed method require in average 750 bytes of storage size. Even though only matching nodes and number of branches per matching node were used in the experiments reported here, additional information about end-points can be used, possibly increasing the reliability and robustness of the representation.

6 Conclusion

This work presented a biometric iris identification method in which morphological operators were used to extract *stable local* patterns to represent and characterise human irises. The morphological approach was used successfully in several processing stages, such as iris localisation, segmentation and local feature extraction.

The fact of using local information to represent irises makes the proposed method very flexible, in such a way that different types of features (nodes, branches and end-points) can be specifically chosen to be used or not. Also, the use of local information allows the selection of stable features among a number of different image samples from the same subject, according to the degree of accuracy desired for classification.

Results of experiments using subsets of images from two widely used iris databases – the University of Bath Iris Image Database and CASIA Iris Image Database – show that the proposed approach is suitable to be used in iris recognition systems and is suitable to be used in images acquired in differing resolutions and under differing illumination conditions.

Statistical analysis of the experiments was based on a method that allows determination of the optimal decision threshold from intraclass and interclass matching

distribution curves. ROC curve analysis and the AUC were used in order to compare the proposed method and Daugman's state-of-the-art method, showing that they achieve equivalent performances despite their rather different processing approaches.

References

1. Boles, W., & Boashash, B. (1998). A human identification technique using images of the iris and wavelet transform. *IEEE Transactions on Signal Processing*, *46*(4), 1185–1188.
2. Bovik, A. (Ed.) (2000). *Handbook of image and video processing. Communications, networking and multimedia*. San Diego: Academic Press.
3. Chinese Academy of Sciences' Institute of Automation (2007). *CASIA iris image database V3*. http://www.cbsr.ia.ac.cn/IrisDatabase.htm.
4. Conti, V., Milici, G., Sorbello, F., Vitabile, S. (2007). A novel iris recognition system based on micro-features. In *Proceedings of the IEEE workshop on automatic identification advanced technologies* (pp. 253–258). Alghero.
5. Daugman, J. (1993). High confidence visual recognition of persons by a test of statistical independence. *IEEE Transactions on Pattern Analysis and Machine Intelligence*, *15*(11), 1148–1161.
6. Daugman, J. (1995). High confidence recognition of persons by video analysis of iris texture. In *Proceedings of the European convention on security and detection* (pp. 244–251). Brighton.
7. Daugman, J. (2001). Statistical richness of visual phase information: update on recognizing persons by iris patterns. *International Journal of Computer Vision*, *45*(1), 25–38.
8. Gonzalez, R., & Woods, R. (1992). *Digital image processing* . Reading: Addison-Wesley.
9. Grabowski, K., Sankowski, W., Napieralska, M., Zubert, M., Napieralski, A. (2006). Iris recognition algorithm optimized for hardware implementation. In *Proceedings of the IEEE symposium on computational intelligence and bioinformatics and computational biology* (pp. 1–5). Toronto.
10. Kennell, L.R., Ives, R.W., Gaunt, R.M. (2006). Binary morphology and local statistics applied to iris segmentation for recognition. In *Proceedings of the 13th international conference on image processing* (pp. 293–296). Atlanta: IEEE Press.
11. Lim, S., Lee, K., Byeon, O., Kim, T. (2001). Efficient iris recognition through improvement of feature vector and classifier. *ETRI Journal*, *23*(2), 61–70.
12. Ma, L., Wang, Y., Tan, T. (2002). Iris recognition based on multichannel gabor filtering. In *Proceedings of the 5th Asian conference on computer vision* (pp. 279–283). Melbourne.
13. Ma, L., Tan, T., Wang, Y., Zhang, D. (2004). Efficient iris recognition by characterizing key local variations. *IEEE Transactions on Image Processing*, *13*(6), 739–750.
14. Mansfield, A., & Wayman, J. (2002). *Best practices in testing and reporting performance of biometric devices*. Tech. rep., Centre for Mathematics and Scientific Computing, National Physical Laboratory, Teddington.
15. Martin-Roche, D., Sanchez-Avila, C., Sanchez-Reillo, R. (2001). Iris recognition for biometric identification using dyadic wavelet transform zero-crossing. In *Proceedings of the 35th IEEE international Carnahan conference on security technology* (pp. 272–277). London.
16. Mira Jr., J., & Mayer, J. (2003). Image feature extraction for application of biometric identification of iris: A morphological approach. In *Proceedings of the 16th Brazilian symposium on computer graphics and image processing*. São Carlos.
17. Monro, D., Rakshit, S., Zhang, D. (2007). DCT-based iris recognition. *IEEE Transactions on Pattern Analysis and Machine Intelligence*, *29*(4), 586–595.
18. Popescu-Bodorin, N., & Balas, V.E. (2010). Comparing Haar-Hilbert and Log-Gabor based iris encoders on Bath Iris Image Database. In *Proceedings of the 4th international workshop on soft computing applications* (pp. 191–196). Arad: IEEE Press.
19. Proença, H., & Alexandre, L. (2007). Toward noncooperative iris recognition: a classification approach using multiple signatures. *IEEE Transactions on Pattern Analysis and Machine Intelligence*, *29*(4), 607–612.
20. Schreiner, K. (1999). Biometrics: prospects for going the distance. *IEEE Intelligent Systems and their Applications*, *14*(6), 2–6.
21. Serra, J. (1984). *Image analysis and mathematical morphology* (Vol. 1). London: Academic.
22. Soille, P. (2003). *Morphological image analysis: Principles and applications*, 2nd edn. New York: Springer.
23. Stiller, C., & Konrad, J. (1999). Estimating motion in image sequences. *IEEE Signal Processing Magazine*, *16*(4), 70–91.
24. University of Bath, Smart Sensors Ltd. (2012). *Bath iris image database*. http://www.smartsensors.co.uk/information/bath-iris-image-database/.
25. Vincent, L. (1992). Morphological area opening and closing for grayscale images. In: *Proceedings of the NATO shape in picture workshop* (pp. 197–208). Driebergen: Springer.
26. Vincent, L. (1993). Morphological grayscale reconstruction in image analysis: applications and efficient algorithms. *IEEE Transactions on Image Processing*, *2*(2), 176–201.
27. Vincent, L. (1997). Current topics in applied morphological image analysis. In W. Kendall, O. Barndorff-Nielsen, M. van Lieshout(Eds.), Current trends in stochastic geometry and its applications. London: Chapman & Hall.
28. Wildes, R. (1997). Iris recognition: an emerging biometric technology. *Proceedings of the IEEE*, *85*(9), 1347–1363.
29. Xu, G.z., Zhang, Z.f., Ma, Y.d. (2008). An image segmentation based method for iris feature extraction. *The Journal of China Universities of Posts and Telecommunications*, *15*(1), 96–101, 117.
30. Ziauddin, S., & Dailey, M.N. (2009). A robust hybrid iris localization technique. In *Proceedings of the 6th international conference on electrical engineering/electronics, computer, telecommunications and information technology* (pp. 1058–1061). Pattaya.
31. Zuo, J., Schmid, N.A., Chen, X. (2007). On generation and analysis of synthetic iris images. *IEEE Transactions on Information Forensics and Security*, *2*(1), 77–90.

Joaquim de Mira Junior obtained his BSc in Electrical Engineering from the Federal University of Itajubá in 1990, his MSc in Electrical Engineering from the Federal University of Santa Catarina (UFSC) in 2003 and his PhD in Biomedical Engineering from the Federal University of Technology - Paraná (UTFPR) in 2012. He is with the Department of Electronics at UTFPR (Ponta Grossa) and his major research interests are in the fields of biometric identification, iris recognition, as well as signal and image processing applied to automation systems.

Hugo Vieira Neto obtained his BSc in Electrical Engineering and his MSc in Applied Computer Science from the Federal University of Technology - Paraná (UTFPR) in 1995 and 1998, respectively, and his PhD in Robotics from the University of Essex in 2006. He has been with the Department of Electronics at UTFPR (Curitiba) since 1998 and with the Biomedical Engineering and Computer Engineering Research Groups at the Graduate School on Electrical Engineering and Applied Computer Science (CPGEI) since 2007. His major research interests are in the fields of computer vision, machine learning and mobile robotics.

Eduardo Borba Neves obtained his BSc in Physical Therapy from University Estácio de Sá in 2002, his MSc in Public Health from the Federal University of Rio de Janeiro (UFRJ) in 2007, his first PhD in Biomedical Engineering from the Federal University of Rio de Janeiro (UFRJ) in 2009, and his second PhD in Public Health and Environment from the Oswaldo Cruz Foundation (FIOCRUZ) in 2011. He is currently with the Graduate Program in Biomedical Engineering (PPGEB) at the Federal University of Technology - Paraná (UTFPR) and his major research interests are in the fields of epidemiology, health assessment technologies, as well as diagnostic and therapeutic technologies.

Fábio Kurt Schneider obtained his BSc in Electrical Engineering and his MSc in Biomedical Engineering from the Federal University of Technology - Paraná (UTFPR) in 1989 and 1995, respectively, and his PhD in Electrical Engineering from the University of Washington in 2006. He has been with the Department of Electronics at UTFPR (Curitiba) since 1995 and with the Biomedical Engineering Research Group at the Graduate School on Electrical Engineering and Applied Computer Science (CPGEI) since 2007. His research interests are in the fields of biomedical signal and image processing, ultrasound imaging, bioinstrumentation, and digital systems design based on high-performance digital signal processors and reconfigurable devices.